Photosensitive Polymeric Materials for Two-Photon 3D WORM Optical Data Storage Systems

Ciceron O. Yanez,[†] Carolina D. Andrade,[†] Sheng Yao,[†] Gheorghe Luchita,[†] Mykhailo V. Bondar,[‡] and Kevin D. Belfield*[,†,§]

Department of Chemistry and CREOL, The College of Optics and Photonics, University of Central Florida, Orlando, Florida 32816, and Institute of Physics, Academy of Sciences of Ukraine, Prospect Nauki 46, Kiev 28, 03028 Ukraine

ABSTRACT We report the photochemistry and development of a fluorescence readout-based, nonlinear absorption, three-dimensional optical data storage system. In this system, writing was achieved by acid generation upon two-photon absorption (2PA) of a photoacid generator (PAG; at 710 or 730 nm). Readout was then performed by interrogating two-photon-absorbing dyes, after protonation, at 860 nm. Linear and nonlinear photophysical characterization of 2PA PAGs and acid-sensitive fluorescent dyes demonstrates good spectral resolution between the PAG and protonated 2PA dye and relatively high two-photon absorptivity. Solution spectroscopic studies confirm photoacid generation and dye protonation. Two-photon recording and readout of voxels were demonstrated in five and eight consecutive, crosstalk-free layers within a polymer matrix, generating a data storage capacity of up to 1.8×10^{13} bits/cm^3.

KEYWORDS: optical data storage • two-photon absorption • photoacid generators • PAGs • fluorescence • two photon

INTRODUCTION

Data are being generated at a remarkably explosive rate. For example, in 2006 alone, 161 exabytes (161 billion gigabytes) of new data were generated worldwide, and this is projected to grow to 1800 exabytes by 2011. The key driving force of future development is expected to be the rapid expansion of the Internet and multimedia, such as high-definition television (HDTV) with their requirements for higher bandwidth and storage capacity. The storage capacities of current optical data storage (ODS) technologies like the compact disk (CD), digital video disk (DVD), and Blu-ray depend on the bit density that can be achieved on the two-dimensional (2D) recording surface. In all of these technologies, this bit density is limited by the Raleigh criterion, which when applied to ODS can be expressed as $D \propto k(S\mathrm{NA}^2/\lambda^2)$, where D is the storage capacity (usually expressed in bytes), S is the effective recording surface, NA is the numerical aperture of the scanning objective used for the writing process, and λ is the wavelength used for recording the information (1). Currently, the capacity of ODS systems has increased by increasing the NA of the scanning objective, decreasing the wavelength of the source, or both. Further changes in these two parameters, beyond what is currently employed by the Blu-ray system (NA = 0.85; λ = 405 nm), are not feasible or are too expensive to be implemented in commercial ODS systems.

To overcome the limitations imposed by the diffraction limit of the wavelength used for writing and readout, new ODS systems have relied on the nonlinear optical properties of their components. The storage capacity advantage that nonlinear absorption-based ODS systems have over their linear counterparts is based on the quadratic dependence of two-photon absorption (2PA) with respect to the intensity of incident light ($dw/dt \propto I^2$). This quadratic dependence of 2PA enables the photochemical or photophysical processes that depend on this absorption to be confined to very small volumes. Hence, this nonlinear dependence leads to an immense data storage capacity (2). Several efforts have been made to further develop both erasable (rewritable) (3) and nonerasable (permanent or write-once read-many, WORM) (2, 4, 5) systems. The increased spatial resolution of nonlinear absorption processes enables true three-dimensional (3D) ODS, and many recent efforts have proven that subdiffraction limit features can be recorded when the 2PA properties of the ODS systems are exploited. A key step in this direction in the ODS field was reported by Parthenopoulos and Rentzepis in 1989 (6). In this work, two-photon writing, erasing, and reading were achieved by the photochromic interconversion of spyrobenzopyrans.

We previously reported a 2D fluorescence readout WORM system where the protonation of a 2PA dye (1) was achieved by using a commercially available photoacid generator (PAG), developed originally for UV curing (4). Because of limited π conjugation, the 2PA cross sections of commercially available PAGs are low (7), significantly hindering the development of this type of ODS system. To increase

* To whom correspondence should be addressed. E-mail: belfield@mail.ucf.edu.
Received for review August 28, 2009 and accepted September 20, 2009
[†] Department of Chemistry, University of Central Florida.
[‡] Academy of Sciences of Ukraine.
[§] CREOL, The College of Optics and Photonics, University of Central Florida.
DOI: 10.1021/am900587u

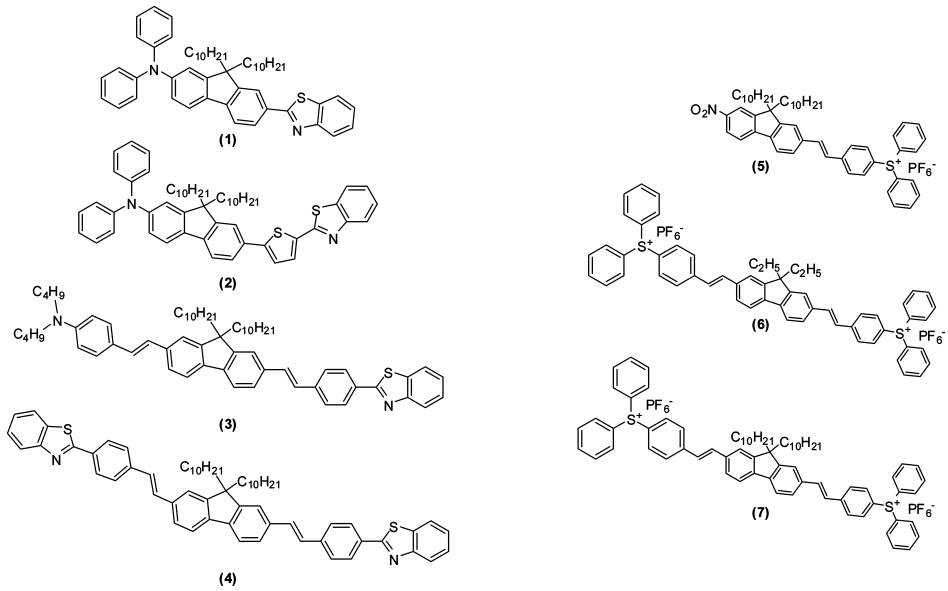

FIGURE 1. 2PA acid-sensitive dyes 1−4 and 2PA sulfonium PAGs 5−7.

Scheme 1. Synthesis of 2PA Dye 3[a]

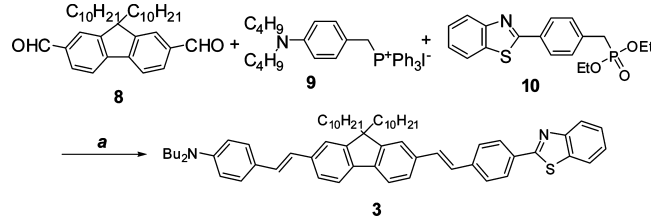

[a] DMF, NaH, rt, 20 h, 43%.

the efficiency of this system, 2PA PAGs with higher cross sections were needed. Herein, we report the use of new photosensitive polymeric systems, comprised of novel, acid-sensitive, two-photon-absorbing dyes **2**−**4** and significantly improved sulfonium PAGs **4**−**6** (Figure 1) in different polymer matrixes. One of these new systems, containing novel PAG **5** and a new two-photon-absorbing dye (**2**), enabled a true 3D (multilayer) WORM ODS where the two-photon advantage is fully exploited. This improved ODS system allowed the two-photon recording and readout of voxels in eight consecutive layers within the polymer matrix, resulting in a crosstalk-free system in which the 3D character of this 2PA ODS was demonstrated.

EXPERIMENTAL SECTION

Materials. The syntheses of fluorescent dyes **1** and **4** and all PAGs are reported elsewhere (8−10). The phosphorylated poly(vinylbenzyl chloride-*co*-methyl methacrylate) [poly(VBC-*co*-MMA), **19**; see Figure 6 for its structure], used as a polymer matrix, was synthesized according to the literature (11). 9,9-Didecyl-9*H*-fluorene-2,7-dicarbaldehyde (**8**) (12), [4-(dibutylamino)benzyl]triphenylphosphonium iodide (**9**) (13), diethyl 4-(benzo[*d*]thiazol-2-yl)benzylphosphonate (**10**) (14), 2-(5-bromothiophen-2-yl)benzothiazole (**11**) (8), and 9,9-didecyl-2-iodo-7-nitro-9*H*-fluorene (**13**) (15) were prepared according to the literature methods. All solvents and monomers were used as received. Masks used during photoexposure of photosensitive polymer films included transmission electron microscopy (TEM) grids (600- and 400-mesh grids from Polysciences) and glass resolution targets (negative slide with a 1951 USAF test pattern from Edmund Scientific).

[4-[2-[7-[2-(4-Benzothiazol-2-ylphenyl)vinyl]-9,9-didecyl-9*H*-fluoren-2-yl]vinyl]phenyl]dibutylamine (3; Scheme 1). A mixture of **8** (0.25 g, 0.5 mmol), **9** (0.30 g, 0.5 mmol), and **10** (0.18 g, 0.5 mmol) in 10 mL of dry *N*,*N*-dimethylformamide (DMF) was degassed by argon for 30 min. NaH (0.24 g, 10.0 mmol) was then added and the mixture stirred at room temperature (rt) under argon for 20 h. The crude product precipitated by the slow addition of water was collected by filtration and purified by column chromatography using hexane/CH_2Cl_2 = 1/3 as the eluent to afford 0.20 g of compound **5** (43% yield). Mp: 95−96 °C. ^{1}H NMR (300 MHz, $CDCl_3$): δ 8.07 (m, 3H, Ph−H), 7.89 (d, J = 7.8 Hz, 1H, Ph−H), 7.63 (m, 4H, Ph−H), 7.51−7.38 (m, 8H, Ph−H), 7.31 (d, J = 16.8 Hz, 2H, CH═), 7.17 (d, J = 16.2 Hz, 2H, CH═), 7.08 (d, J = 16.2 Hz, 2H, CH═), 6.95 (d, J = 16.2 Hz, 2H, CH═), 6.62 (d, J = 8.1 Hz, 2H, Ph−H), 3.29 (m, 4H, NCH_2), 2.02 (m, 4H, CH_2), 1.58 (m, 4H, CH_2), 1.37 (m, 4H, CH_2), 1.15−1.06 (m, 28H, CH_2), 0.97 (t, J = 7.1 Hz, 6H, CH_3), 0.82 (t, J = 5.9 Hz, 6H, CH_3), 0.68 (m, 4H, CH_2). ^{13}C NMR (75 MHz, $CDCl_3$): δ 154.29, 151.60, 147.85, 141.59, 140.47, 139.51, 137.70, 135.54, 135.13, 132.43, 131.33, 128.54, 128.05, 127.89, 127.02, 126.70, 126.49, 126.08, 125.26, 124.79, 124.35, 123.28, 121.77, 121.08, 120.31, 120.09, 119.93, 111.81, 55.31, 51.18, 40.98, 32.32, 32.05, 30.54, 30.08, 30.01, 29.95, 29.74, 24.25, 23.13, 20.86, 14.62, 14.53. Anal. Calcd for $C_{64}H_{82}N_2S$ (911.42): C, 84.34; H, 9.07; N, 3.07. Found: C, 84.34; H, 9.28; N, 3.08.

Synthesis of 7-(5-(Benzothiazol-2-yl)thiophen-2-yl)-9,9-didecyl-*N*,*N*-diphenyl-9*H*-fluoren-2-amine (2). The transformation of benzothiazole derivative **11** into tin derivative **12** and the subsequent palladium-catalyzed Stille coupling with the key fluorene intermediate **13** was accomplished, as shown in Scheme 2, by using methodology previously reported by our group, affording compound **14** in excellent yield. The reduction

Scheme 2. Synthesis of 2PA Dye 2[a]

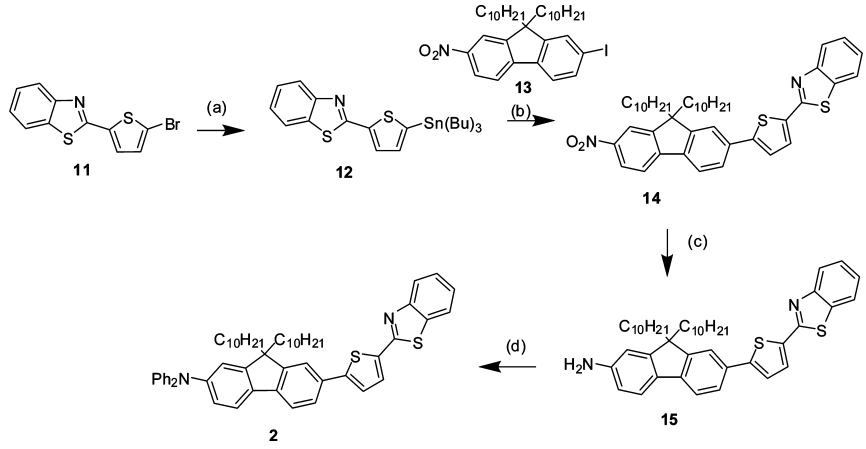

[a] (i) THF, −78 °C, $Sn(Bu)_3Cl$, 1 h; (ii) (a) rt, overnight, 70%; (b) toluene, $Pd(PPh_3)_2Cl_2$ reflux, 5 h, 98%; (c) THF/EtOH = 1/1, $NH_2NH_2 \cdot 2H_2O$, 10% Pd/C, 70 °C, 20 h, 84%; (d) 1,2-dichlorobenzene, iodobenzene, copper−bronze, 18-crown-6, K_2CO_3, 180 °C, 48 h, 94%.

of the nitrofluorene derivative **14** and posterior reaction of amine **15** with iodobenzene under Ullmann conditions generated the D−π−A-type fluorescent dye **2**.

Synthesis of 2-(5-(Tributylstannyl)thiophen-2-yl)benzothiazole (12). At −78 °C, **11** (200 mg, 0.67 mmol) was dissolved in dry tetrahydrofuran (THF; 5 mL). A solution of *n*-BuLi in hexanes (0.27 mL, 2.5 M, 0.68 mmol) was added dropwise into the reaction mixture. After stirring for 1 h, $Sn(Bu)_3Cl$ (360 mg, 1.10 mmol) was added, and the mixture was allowed to reach room temperature and stirred overnight. The mixture was added to water, extracted with Et_2O twice, dried over Mg_2SO_4, and purified by column chromatography, using a mixture of hexane/ethyl acetate (9:1) as the eluent, to yield 240 mg (70%) of viscous oil. ^{1}H NMR (500 MHz, $CDCl_3$): δ 8.02 (d, J = 8.2 Hz, 1H, Ph−H), 7.82 (d, J = 8.0 Hz, 1H, Ph−H), 7.74 (d, J = 3.5 Hz, 1H, Ar−H), 7.45 (m, 1H, Ph−H), 7.33 (m, 1H, Ph−H), 7.18 (d, J = 3.5 Hz, 1H, Ar−H), 1.59 (m, 6H, CH_2), 1.35 (m, 6H, CH_2), 1.16 (m, 6H, CH_2), 0.90 (t, J = 7.34 Hz, 9H, CH_3). ^{13}C NMR (125 MHz, $CDCl_3$): δ 161.40, 153.85, 143.46, 142.35, 136.18, 134.70, 129.60, 126.23, 125.06, 122.85, 121.44, 28.94, 27.28, 13.72, 10.98. Anal. Calcd for $C_{23}H_{33}NS_2Sn$: C, 54.56; H, 6.57; N, 2.77. Found: C, 54.85; H, 6.67; N, 2.86.

Synthesis of 2-(5-(9,9-Didecyl-7-nitro-9*H*-fluoren-2-yl)thiophen-2-yl)benzothiazole (14). 13 (200 mg, 0.32 mmol), **12** (191 mg, 0.38 mmol), and $Pd(PPh_3)_2Cl_2$ (6 mg, 0.008 mmol) were dissolved in toluene (4 mL). The mixture was heated under reflux for 5 h. The solvent was removed under reduced pressure, and the crude was purified by column chromatography, using a mixture of hexane/ethyl acetate (9.5:0.5) as the eluent, to yield 222 mg (98%) of a yellow oil that solidified upon standing. Mp: 73.2−74.9 °C. ^{1}H NMR (500 MHz, $CDCl_3$): δ 8.28 (dd, J = 8.3 and 2.0 Hz, 1H, Ph−H), 8.22 (d, J = 2.0 Hz, 1H, Ph−H), 8.05 (d, J = 8.0 Hz, 1H, Ph−H), 7.88 (d, J = 7.8 Hz, 1H, Ph−H), 7.82 (m, 2H, Ph−H), 7.74 (m, 1H, Ph−H), 7.69 (d, J = 1.4 Hz, 1H, Ph−H), 7.66 (d, J = 3.7 Hz, 1H, Ar−H), 7.50 (m, 1H, Ph−H), 7.46 (d, J = 3.7 Hz, 1H, Ar−H), 7.39 (m, 1H, Ph−H), 2.06 (m, 4H, CH_2), 1.09 (m, 28H, CH_2), 0.82 (t, J = 7.0 Hz, 6H, CH_3), 0.62 (m, 4H, CH_2). ^{13}C NMR (125 MHz, $CDCl_3$): δ 160.97, 153.69, 153.38, 152.20, 147.89, 147.24, 146.80, 139.03, 136.59, 134.68, 134.37, 129.48, 126.59, 125.29, 124.40, 124.36, 123.45, 122.95, 121.84, 121.51, 120.43, 119.97, 118.28, 55.87, 40.07, 31.84, 29.83, 29.49, 29.47, 29.24, 29.19, 23.78, 22.63, 14.08. Anal. Calcd for $C_{44}H_{54}N_2O_2S_2$: C, 74.74; H, 7.70; N, 3.96. Found: C, 74.97; H, 7.85; N, 3.97.

Synthesis of 7-(5-(Benzothiazol-2-yl)thiophen-2-yl)-9,9-didecyl-9*H*-fluoren-2-amine (15). 14 (160 mg, 0.23 mmol) and 10% Pd/C (16 mg) were dissolved in a 1:1 mixture of THF/EtOH (8 mL). $NH_2NH_2 \cdot 2H_2O$ (136 mg, 2.7 mmol) was added to the mixture slowly at room temperature, and then the resulting mixture was heated to 70 °C for 20 h. The mixture was filtered though a silica plug with CH_2Cl_2, and after removal of the solvent under reduced pressure, the crude product was purified by column chromatogrtaphy, using a mixture of hexane/ethyl acetate (9:1) as the eluent, to yield 130 mg (84%) of a dark-yellow oil. Because of the sensitivity of the amine, **15** was used directly in the next step. ^{1}H NMR (500 MHz, $CDCl_3$): δ 8.04 (d, J = 8.0 Hz, 1H, Ph−H), 7.85 (d, J = 8.0 Hz, 1H, Ph−H), 7.61 (m, 2H, Ph−H), 7.56 (m, 2H, Ph−H), 7.48 (m, 2H, Ph−H), 7.36 (m, 2H, Ar−H), 6.67 (m, 2H, Ph−H), 3.79 (s, 2H, NH_2), 1.91 (m, 4H, CH_2), 1.11 (m, 28H, CH_2), 0.83 (t, J = 7.0 Hz, 6H, CH_3), 0.67 (m, 4H, CH_2). ^{13}C NMR (125 MHz, $CDCl_3$): δ 161.38, 153.75, 153.11, 150.74, 149.56, 146.40, 142.35, 135.01, 134.60, 131.62, 130.45, 129.54, 126.42, 125.05, 124.69, 123.02, 122.78, 121.42, 120.81, 120.06, 118.76, 114.05, 109.65, 54.93, 40.62, 31.87, 30.09, 29.63, 29.53, 29.29, 29.28, 23.75, 22.65, 14.10.

Synthesis of 2. 15 (130 mg, 0.19 mmol), iodobenzene (157 mg, 0.77 mmol), copper−bronze (61 mg, 0.96 mmol), 18-crown-6 (15 mg, 0.058 mmol), and K_2CO_3 (212 mg, 1.54 mmol) were combined with 1,2-dichlorobenzene (3 mL). The mixture was heated to 180 °C for 48 h. The product was passed through a silica plug with CH_2Cl_2. The solvent was removed under reduced pressure, and the crude product was purified by column chromatography on silica gel, using a mixture of hexane/ethyl acetate (9:1) as the eluent, to yield 150 mg (94%) of a yellow solid. Mp: 107.5−109.5 °C. ^{1}H NMR (500 MHz, $CDCl_3$): δ 8.04 (d, J = 8.0 Hz, 1H, Ph−H), 7.84 (d, J = 8.0 Hz, 1H, Ph−H), 7.62 (m, 4H, Ph−H), 7.56 (d, J = 8.0 Hz, 1H, Ph−H), 7.47 (m, 1H, Ph−H), 7.35 (m, 2H, Ar−H), 7.26 (m, 5H, Ph−H), 7.14 (m, 5H, Ph−H), 7.02 (m, 2H, Ph−H), 1.91 (m, 4H, CH_2), 1.12 (m, 28H, CH_2), 0.85 (t, J = 7.0 Hz, 6H, CH_3), 0.70 (m, 4H, CH_2). ^{13}C NMR (125 MHz, $CDCl_3$): δ 161.31, 153.75, 152.48, 151.63, 149.22, 147.88, 147.53, 141.61, 135.37, 134.63, 131.38, 129.57, 129.49, 129.24, 129.16, 125.16, 125.02, 123.97, 123.91, 123.37, 123.29, 122.84, 122.64, 121.47, 121.43, 120.10, 104.99, 55.18, 40.24, 31.91, 30.00, 29.61, 29.57, 29.32, 23.87, 22.67, 14.12. Anal. Calcd for $C_{56}H_{64}N_2S_2$: C, 81.11; H, 7.78; N, 3.38. Found: C, 80.81; H, 7.74; N, 3.30.

One-Photon Recording and Readout. One-photon recording was carried out by irradiating the photoreactive polymer with a Loctite 97034 light source equipped with a 200 W mercury lamp and an internal shutter to control the exposure times. The photomask was either projected or placed (as a contact mask) on the dry polymeric film. Output from the waveguide of the light source was focused into the condenser of an Olympus IX-81 confocal microscope. One-photon fluorescence images were

recorded on this microscope, which was equipped with a Hamamatsu EM-CCD C9100 digital camera. One-photon confocal fluorescence images for readout were taken using a FITC filter cube (Ex:477/50; DM: 507; Em:536/40) and a modified TRITC filter cube (Ex:525/40; DM: 555; Em:624/40) for the neutral and protonated forms of the dyes, respectively.

Photosensitive polymer films were solution-cast onto 2.5 × 2.5 cm microscope glass coverslips. The film thickness of the polymer films was approximated by focusing on the glass surface and then on the upper surface of the polymer and determining the distance the *z* stage traveled from one surface to the other.

Two-Photon Recording and Readout. Two-photon recording and readout were performed on a modified Olympus Fluoview FV300 laser scanning confocal microscopy system equipped with a broad-band, tunable Coherent Mira Ti:sapphire laser (recording at 730 or 760 nm; readout at 860 nm, 115 fs pulse width, 76 MHz repetition rate), pumped by a 10 W Coherent Verdi frequency-doubled Nd:YAG laser. In two-photon writing, the exposure time and position were controlled by means of an electronic shutter and electronic stage, respectively, both from Thor Laboratories.

Spectra. Absorption spectra were recorded with an Agilent 8453UV−vis spectrophotometer. Steady-state fluorescence spectra were measured with a PTI Quantamaster spectrofluorimeter.

Fluorescence Quantum Yield Measurements. Fluorescence quantum yields were determined relative to 9,10-diphenylanthracene in cyclohexane as the standard (16). Measurements were made in the photon-counting regime of a PMT using an L-format configuration using a PTI Quantamaster spectrofluorimeter. The fluorescence spectra were corrected for the spectral dependence of the PMT. All measurements were performed at room temperature in 1 cm quartz cuvettes with dye concentrations on the order of 10^{-6} M.

Photoacid Quantum Yield Measurements. Steady-state photoacid quantum yields were measured by selectively exciting PAG solutions at the desired wavelength using the monochromator of the PTI spectrofluorimeter. Irradiance of the incident radiation was measured with an Ophir Power Star power meter equipped with a UV 1.44 cm^2 detector head. Rhodamine B was used as a sensor of photoacid generation, observing that the change in the optical density of the sulfonium salt did not exceed 5% (17). Photoacid quantum yields were calculated by means of the following expression:

$$\Phi_{\lambda}^{H+} = \frac{\dfrac{\Delta OD^{555\,nm}}{\varepsilon_{555\,nm}^{RhB} dV_{sol}} N}{\Delta S I_0 \Delta t (1 - 10^{-OD_0})} \qquad (1)$$

where $\Delta OD^{555\ nm}$ is the change in the optical density upon generation of rhodamine B measured at 555 nm, $\epsilon^{RhB}{}_{555}$ is the extinction coefficient of rhodamine B at 555 nm in acetonitrile, *d* is the irradiation path length (typically 1 cm) of cuvette, ΔS is the area of the irradiated solution (photon flux area), Δt is the irradiation time, and OD_0 is the average absorption intensity (which did not change by more than 0.5% at any given time). The quantum yield of photoacid generation of triphenylsulfonium tetrafluoroborate was determined by this method ($\Phi^+ = 0.57$) and was comparable to the literature value (0.54) (11). PAG solutions were on the order of 10^{-5} M in acetonitrile.

2PA Cross Section Measurements. 2PA cross sections of the PAGs and fluorescent dyes were determined by the two-photon-induced fluorescence method (18). A tunable Mira 900-F femtosecond Ti:sapphire laser pumped by a Verdi V-10 frequency-doubled Nd:YAG laser (Coherent) was used as the excitation source, and a PTI Quantamaster spectrofluorimeter with PMT detectors was used for measurement. The linear polarization and power of the laser light were adjusted by an optical attenuator consisting of two Glan−Thompson polarizers and a half-wave plate. The laser beam was divided with a beam splitter from where the transmitted beam was expanded with a beam expander and passed through the sample after being focused with an objective lens. The reflected beam was sent to the power meter to monitor the variation of the incident power on the sample. The upconverted fluorescence was collected by the PMT of the PTI Quantamaster spectrofluorimeter at a direction perpendicular to the pump beam. The numerical estimation of the 2PA cross sections δ was performed by comparison with a known reference using eq 2:

$$\delta = \delta_R \frac{\langle I \rangle}{\langle I_R \rangle} \frac{C_R}{C} \frac{n^2}{n_R{}^2} \frac{Q_R}{Q} \frac{P_R{}^2}{P^2} \qquad (2)$$

where the subscript R refers to the reference, $\langle I \rangle$ is the integrated intensity from two-photon excitation, *C* is the concentration, *n* is the refractive index, *Q* is the quantum yield, and *P* is the incident power on the sample. All spectra were corrected for the spectral responsivity of a PTI detection system. Follow-up fluorescence spectra after each measurement ensured that the exposure during the experiment did not induce photodecomposition greater than 0.5% for any of the 2PA molecules.

RESULTS AND DISCUSSION

System. The ODS system is composed of an acid-sensitive fluorescent dye, a PAG, and a polymer substrate. Information recording or writing in the ODS system was achieved by the monoprotonation of the 2PA fluorescent dye upon photogeneration of H^+. For example, when dye **1** was used, the benzothiazole nitrogen was protonated when the corresponding PAG was exposed by one- or two-photon irradiation. Irradiation of localized volumes within the polymer matrix, where the sulfonium salt is found in ≈5% (w/w), induced the generation of hexafluorophosphoric acid. In the particular case of dye **1**, because the pK_b of the benzothiazole nitrogen (pK_b≈13) (19) is lower than that of the diphenylamino nitrogen functionality (pK_b≈19) (20), the benzothiazole nitrogen was the first to be protonated upon production of superacid. The monoprotonated species of the 2PA dye exhibited a large bathochromic shift in the absorption spectrum (Figure 2, **1a**), due to the increase of the electron-withdrawing character of the protonated benzothiazole. Hence, emission of the monoprotonated form is at longer wavelengths than that of the unexposed, neutral form of the dye (4). Nonprotonated **1** and protonated **1a** can be interrogated for readout, enabling positive and negative images when addressing the exposed polymer at shorter or longer wavelengths, respectively (i.e., at a short-wavelength readout, one excites the nonprotonated dye, resulting in short-wavelength emission while one can irradiate the protonated dye at longer wavelength, resulting in a long-wavelength emission for two-channel readout). Longer-wavelength readout had the advantage that the photoacid was unaffected at these wavelengths, resulting in a nondestructive readout. All three components of the ODS system were evaluated: 2PA dye, polymer matrix, and 2PA PAG.

2PA Fluorescent Dyes. ***Spectroscopic Studies in Solution.*** The dyes that were tested had nitrogens of

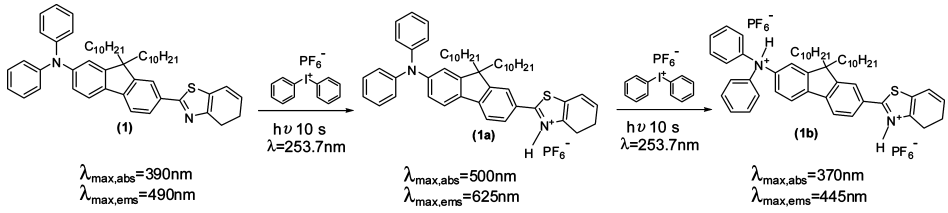

FIGURE 2. Protonation of 2PA fluorescent dye 1 in an acetonitrile solution with an excess of diphenyliodonium hexafluorophosphate. Exposure to 254 nm radiation produces an increase of the photoacid concentration, inducing dye protonation.

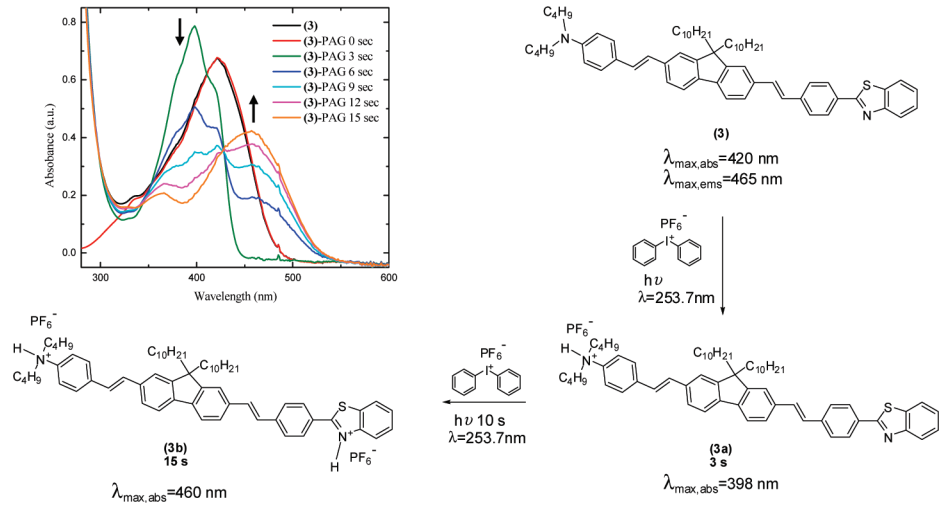

FIGURE 3. Spectral changes of 3 in an acetonitrile solution with diphenyliodonium hexafluorophosphate upon irradiation at 254 nm. Equilibrium of species 3 and 3a at 0−3 s of irradiation. Equilibrium of species 3a and 3b at 3−15 s of irradiation.

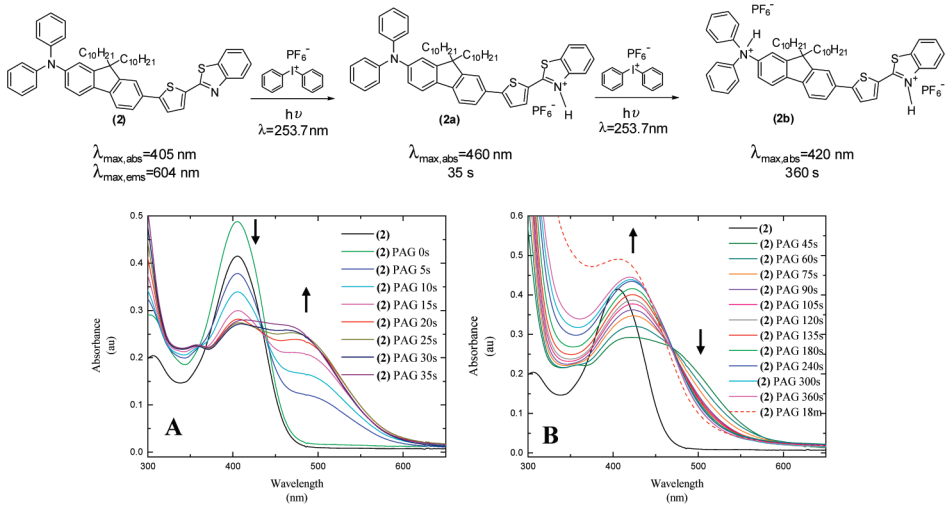

FIGURE 4. Spectral changes of 2 in an acetonitrile solution with diphenyliodonium hexafluorophosphate (PAG) upon irradiation at 254 nm. (A) Equilibrium of species 2 and 2a at 0−35 s of irradiation. (B) Equilibrium of species 2a and 2b at 45 s to 18 min of irradiation.

varying basicity that can undergo protonation upon generation of the photoacid and, as a consequence, change their absorption and emission properties. Besides amines, the only other scaffold that has been used for nonlinear WORM ODS systems with a PAG has been lactones (rhodamine B base) that have been interrogated upon ring opening (5). To assess the advantages and disadvantages of using systems with a more basic *N*,*N*-dibutylaniline moiety (instead of triarylamine) for writing and readout, dye **3** was characterized and evaluated. Spectrophotometric absorption studies of **3** in solution with diphenyliodonium hexaflourophosphate show an initial, rapid blue shift of the absorption λ_{max} of this dye after 3 s of irradiation (Figure 3, **3a**), due to protonation of the *N*,*N*-dibutylaniline moiety, as demonstrated by ^{1}H NMR and COSY studies (not shown). This blue shift was followed by a progressive red shift, due to the formation of species **3b**, which facilitated recording and image readout from both channels (shorter and longer wavelengths). As can be seen in Figure 3, the highest concentration in solution of the protonated species **3b** was reached after 15 s of irradiation. Overexposure leads to a hypsochromic shift, resulting in a species with an absorption λ_{max} of approximately 330 nm. Interrogating this blue-shifted species would result in destructive readout because either the absorption or fluo-

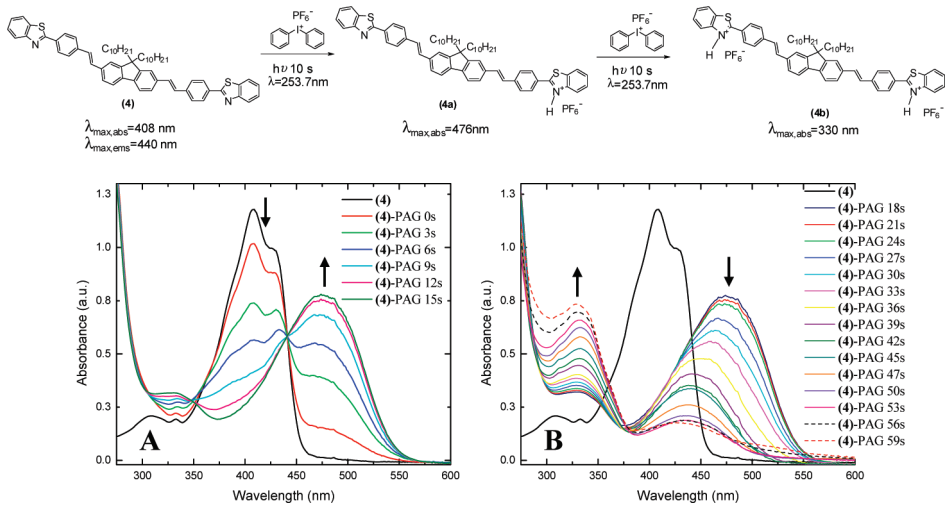

FIGURE 5. Spectral changes of 4 in an acetonitrile solution with diphenyliodonium hexafluorophophate (PAG) upon irradiation at 254 nm. (A) Equilibrium of species 4 and 4a at 0−15 s of irradiation. (B) Equilibrium of species 4a and 4b at 18−59 s of irradiation.

rescence spectra would overlap with the spectrum of the PAG, likely inducing the photoacid generation. Furthermore, the 2PA wavelength would be below the output window (700−1000 nm) of commercial Ti:sapphire femtosecond laser systems. Despite these limitations, the versatility of the system allowed recording and readout, via one-photon absorption (1PA), in both channels (Figure 6).

The behavior of dyes containing aromatic amines as a donor and benzothiazole as an electron-acceptor moiety (D−π−A), such as **1** and **2**, is more predictable because the benzothaizole nitrogen is slightly more basic and will be the first to protonate once the acid is generated upon irradiation, yielding, e.g., species **2a**. Solution studies of dye **2** (Figure 4) indicated that overexposure resulted in less of a blue shift upon generation of diprotonated species **2b**. This effect gave the system greater tolerance to excessive irradiation time and power because species **2a** and **2b** can both be interrogated at wavelengths at which the PAGs will not absorb. Furthermore, the absorption band profile of species **2a** extended beyond 600 nm; this ultimately enabled effective 2PA readout at longer wavelengths (860 nm; see below), where 2PA of the PAG was negligible.

The symmetrical A−π−A system of dye **4** was quickly converted to a D−π−A structure upon photoacid generation, as shown by Figure 5, generating species **4a**. The clear transitions observed in solution studies reveal the protonation of one benzothiazole group, generating a bathochromic shift due to the increased electron-withdrawing properties of the protonated benzothiazole, followed by protonation of the second benzothaizole and the subsequent hypsochromic shift, generating species **4b**. This dye, however, presented solubility problems within the polymer matrix. At concentrations higher than 1.5% (w/w), the dye molecules crystallized, generating scattering domains that significantly affected the optical quality of the polymer film.

Photophysical Properties. The 2PA cross sections of the fluorescent unprotonated dyes ranged between 28 and 1550 GM at 730 nm and between 0 and 550 GM at 860 nm (Table 1). As discussed for the PAGs, the 2PA cross

Table 1. Fluorescence Quantum Yields (Φ_F) and 2PA Cross Sections (δ) of 2PA Dyes 1−4 (Measured in Hexane Except for 3, Which Was Measured in Cyclohexane)

compound	Φ_F*	$\delta_{730\ nm}$ (GM)	$\delta_{760\ nm}$(GM)	$\delta_{860\ nm}$(GM)
1	0.61 ± 0.05	28 ± 5[a]	54 ± 6[a]	<20[a]
2	0.86 ± 0.05	248 ± 25	193 ± 19	132 ± 13
3	1.00 ± 0.05	464 ± 46	238 ± 71	316 ± 32
4	1.00 ± 0.05	1550 ± 155[b]	1450 ± 145[b]	550 ± 55[b]

[a] Reference 21. [b] Reference 9.

section values and the fluorescence quantum yields are key parameters for the 2PA fluorescent dyes in these ODS systems. However, other properties discussed above such as (1) the immediate red shift upon protonation and (2) resilience of the dye to blue shift when excess acid is generated due to overexposure are also important. Consideration of all photophysical properties (high 2PA cross sections, high fluorescence quantum yields, an immediate red shift upon protonation, and minimal shift of the dye upon overexposure) were all considered, leading to the preference of dye **2** over **1**, **3**, and **4** during development of the final system.

Polymer Matrix. Three different polymer matrixes were used as supports. Phosphorylated poly(VBC-*co*-MMA) (**19** in Figure 6) is a highly transparent, robust matrix in which all of the dyes (except **4**) and the PAGs were very soluble. However, this matrix required the use of solvents to help dissolve all of the system components for casting the polymers onto glass slide supports. The solvents must be low-vapor-pressure solvents to ensure that a bubble-free film will be produced after solvent drying. Ultimately, this translates into film-drying procedures that can be fairly lengthy; thus, alternative processing and polymers were explored.

To expedite the film-drying process, creation of a polymer matrix from liquid monomers that can dissolve both the 2PA dye and PAG was investigated. Two thiolene polymer substrates were prepared from the photo-cross-linking of enes **16** and **17** with different proportions of thiol **18** (Figure 6),

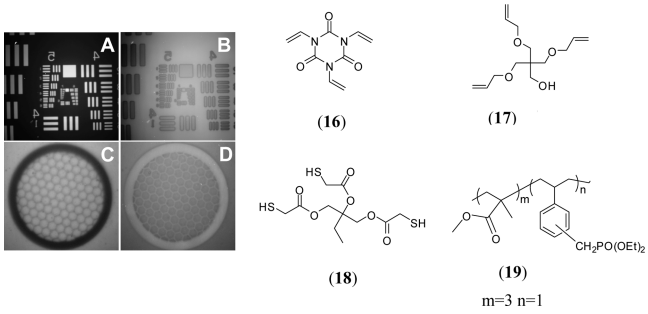

FIGURE 6. One-photon writing and readout images with contact (A and B) and projection (C and D) photomasks. Composition (w/w): 6, 12%; 3, 1.3%; 16, 25%; 17, 25%; 18, 50%. Exposed at 254 nm (3 min) to form a film. Later exposed at 300−400 nm (40 s) for image recording.

in the presence of a free-radical photoinitiator (Irgacure 184), and doped with the PAG/dye mixture. Even though thiolene-cross-linked polymer matrixes are formed by a free-radical-initiated mechanism, these reactions are typically not sensitive to oxygen. Furthermore, many different mechanical and viscoelastic properties of the resulting polymer can be obtained by tailoring the structure and proportions of the monomers (22). Special care was taken in choosing the free-radical photoinitiator to have one with an appropriate λ_{max} so as to not generate photoacid during the formation of the polymer film. The films were made in 3−10 min, and images were successfully recorded and read out on both channels (Figure 6). The FITC filter cube of the confocal microscope was equipped with an excitation bandpass filter (452−502 nm), a dichroic mirror (507 nm), and an emission bandpass filter (496−556 nm) that allowed fluorescence readout of the nonprotonated dye where the resist (polymer composite) remained unexposed. A modified TRITC filter cube, equipped with an excitation bandpass filter (505−545 nm), a dichroic mirror (555 nm), and an emission bandpass filter (604−644 nm), was used to capture the fluorescence of the exposed protonated form of **3**.

2PA PAGs. Because commercially available PAGs are not conjugated enough to generate photoacid by 2PA in the tuning window of Ti:sapphire lasers (700−1000 nm) and because their 2PA cross sections are low, the PAGs used in this system were designed to have high 2PA cross sections at wavelengths accessible to a Ti:sapphire laser system. The PAGs used were prepared as we previously reported (10). It has been observed that symmetrical and unsymmetrical conjugated systems with two electron-donating groups (D) or electron-accepting subtituents (A) tend to have significant two-photon absorptivity (23−25). On the basis of the high thermal and photochemical stabilities of the fluorenyl π system (26), fluorene was chosen as the core structure during the design of the PAGs. Because fluorene can be readily substituted in its 2, 7, and 9 positions, a stilbene or thiophene motif was introduced (2 and 7 positions) to provide additional π conjugation.

In an attempt to increase the photoacid generation efficiency per molecule, two sulfonium salt motifs were introduced in the original model compounds, **6** and **7**, which exhibited an A−π−A architecture. However, the high fluorescence efficiencies of these molecules, as demonstrated by their high fluorescence quantum yield values, hindered the efficiency of photoacid generation (Table 2). The direct photolysis of triarylsulfonium salts has been reported to occur mainly from the singlet state. However, sensitization studies have shown that the triplet triarylsulfonium salts are also labile (27). Consequently, we incorporated a nitro group in the architecture of PAG **5** to quench the fluorescence of the PAG by inducing intersystem crossing and increasing the photoacid quantum yield.

The elimination of the radiative decay pathway was demonstrated by a dramatic decrease in the florescence quantum yield of **5** relative to **7**. The photoacid quantum yield of PAG **5** (Table 2) showed a significant improvement in the photoacid generation efficiency when compared to PAG **7**, indicating that the introduction of groups that favor intersystem crossing, such as functionalities that permit spin−orbital coupling (e.g., the nitro group), is a viable mechanism for increasing the photoacid quantum yield of highly fluorescent triarylsulfonium salt PAGs. The photoacid quantum yields were determined by a steady-state method. The solutions of the PAGs in acetonitrile were selectively irradiated at the desired wavelength with an excitation source of a spectrofluorimeter. Rhodamine B was used as a sensor for photoacid generation as reported by Scaiano et al. (17). Special care was taken in observing a photodecomposition conversion no greater than 5% in order to restrict secondary photoproduct acid generation.

The 2PA cross sections, however, were found to be up to 5 times higher for PAG **7** than for PAG **5** (Table 2). This disparity in 2PA cross section values vs photoacid quantum yield values makes it difficult to rank these PAGs by their overall efficiencies. Using only one of these two photophysical properties would be incomplete and could lead to erroneous interpretations. A more accurate value to compare these PAGs is the 2PA action cross section of photoacid generation, given by the product of photoacid generation quantum yield and the 2PA cross section at a specific wavelength. On the basis of the 2PA action cross section, the overall efficiency of PAG **5** was higher than that of PAG **7**. Hence, the former was chosen as the preferred PAG in the development of the 2PA ODS system.

One-Photon vs Two-Photon Writing and Readout. The advantage of using 2PA dyes is clearly evidenced in the initial two-photon readout experiments (Figure 7), in which the images were recorded by projecting the image of a 600-mesh TEM grid onto the photoreactive polymer surface using a 200 W mercury lamp as the irradiation source. After the image was recorded by 1PA, the fluorescent image was collected by both 1PA and 2PA. The two-photon, upconverted fluorescence image (readout) proved to be much more forgiving to film defects when compared to the one-photon readout, perhaps because of less scattering when longer excitation wavelengths are employed. Furthermore, the inherent nonlinearity of the 2PA system allowed better contrast and sharper images than the one-photon readout (Figure 7a). Scanning across the line indicated on

Table 2. Photophysical Characterization of PAGs 5 and 7

compound	Φ_F[a]	Φ_{H^+}[b]	ϵ_0[c] (M^{-1} cm^{-1})	$\delta_{710\ nm}$ (GM)	$\delta_{730\ nm}$ (GM)	$\delta_{760\ nm}$ (GM)	$\Phi_{H^+}\delta_{710\ nm}$ (GM)
5	0.10 ± 0.01	0.40 ± 0.04	51 000 ± 5000[1]	240 ± 24	80 ± 8	60 ± 6	96 ± 10
7	0.80 ± 0.06	0.03 ± 0.0005	73 000 ± 5000[2]	1275 ± 130	350 ± 35	115 ± 12	38 ± 4

[a] Fluorescence quantum yields, Φ_F, with diphenylanthracene in cyclohexane as the standard; [b] Φ_{H^+} photoacid quantum yields at 350 nm with RhB^+ as the indicator. [c] ϵ_0 molar aborptivity coefficients in acetonitrile at [1]380 nm and [2]400 nm; δ = two-photon absorption cross sections measured at the three different wavelenths used for writing; $\Phi_{H^+}\delta_{710\ nm}$ = two-photon action cross section of photoacid generation at 710 nm.

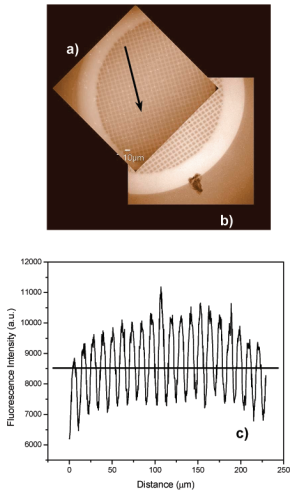

FIGURE 7. Readout images using a TEM 600-mesh projection mask of a mixture of dye 1 and PAG 5 in phosphorylated poly(VBC-*co*-MMA): (a) one-photon readout (FITC 40X readout 20 ms, writing 180 s); (b) two-photon readout (40×, 800 nm, 2 mW, 510IF-550RIF); (c) fluorescence intensity profile for one-photon fluorescence readout when traced along the arrow indicated in part a.

the one-photon readout images afforded the fluorescence intensity scan in Figure 7c. A threshold can be established over which any fluorescence signal can be translated into a binary digital signal. The full width at half-maximum (fwhm) of the fluorescence intensity scan peaks was used to estimate the minimum size feature (ca. 3 μm) for one-photon recording with two-photon readout.

The advantage of using 2PA for writing and readout in all three dimensions of the polymer matrix was demonstrated by an experiment in which voxels were recorded by 2PA in five layers using 730 nm to induce the photoacid generation by 2PA of PAG **5**. An electronic shutter was programmed to open for 50 ms at 10 μm intervals in the x and y axes. After an $x-y$ layer of voxels was recorded (60×, 1.4 NA oil immersion objective), the microscope objective was moved ca. 4 μm to focus deeper into the polymer matrix, generating another layer of voxels. To ensure that the entire depth of the polymer matrix was used for recording, this process was repeated until the objective focal point had well cleared the polymer matrix. After recording, the voxels were read out by both one- and two-photon excitation. One-photon readout was performed by taking a series of confocal fluorescence pictures of the recorded volume at consecutive focal planes of the objective separated by a distance of 0.4 μm. Similarly, the two-photon upconverted fluorescence readout was performed by scanning consecutive 0.4 μm layers of the polymer film at 860 nm in order to excite protonated 2PA dye **2**.

The one-photon confocal fluorescence images were taken using a FITC filter cube (Ex:477/50; DM: 507; Em:536/40) and a modified TRITC filter cube (Ex:525/40; DM: 555; Em: 624/40). One- and two-photon fluorescence intensity vs distance (μm) graphs were then recorded for each voxel layer in order to compare the readout quality obtained by each of the readout methods (Figure 8, one-photon readout; Figure 9, two-photon readout). Clearly, the signal-to-noise ratio in the one-photon readout fluorescence intensity profile is significantly attenuated as one focuses deeper into the polymer film (Figure 8). In the case of two-photon readout (Figure 9), the fluorescence signal readout shows well-defined voxels and comparable, consistently good signal-to-noise ratios for all five layers throughout the entire polymer matrix, a testament of the two-photon advantage. Furthermore, the nonlinearity of the system ensured a crosstalk-free system (Figure 10).

A reconstruction of the 3D image of these voxels was obtained by overlaying all five layers of the upconverted fluorescence images using SlideBook 4.1 (Figure 10A). This reconstruction reveals the absence of crosstalk between voxels within a layer and, importantly, between the layers, illustrating the potential of this system for 3D data storage. The fluorescence intensity scans (from Figure 9C) were normalized and shown in Figure 10B to illustrate how consistent the signal-to-noise ratio is from layer to layer. The size of the voxels is not yet optimized and can be further reduced to increase the storage density of the system.

Once the conditions were optimized for writing and readout, in terms of exposure times and laser beam profile, even smaller voxels were obtained. The reduction of the feature size facilitated recording and readout of eight crosstalk-free layers of voxels (Figures 11, 12, and S1 in the Supporting Information). Though the voxels are difficult to visualize in the figure (Figure 11B), one can easily observe the fluorescence signals in the fluorescence intensity plots in Figure 11C. The average voxel size in these layers was estimated to be 200 nm in radial diameter and 600 nm in axial diameter (Figure 12), as determined by surveying the average size of the voxels in layers 3 and 4 of the eight-layer series. On the basis of this feature size, we estimated the maximum storage capacity to be approximately 1.8×10^{13} bits/cm^3.

CONCLUSIONS

The ODS system proved to be versatile enough to tolerate a wide range of pK_b's of the two-photon-absorbing dyes. A wide variety of architectures can be used as the dye, as long as these dyes exhibit an appreciable bathochromic shift upon acid generation, along with possessing high 2PA cross

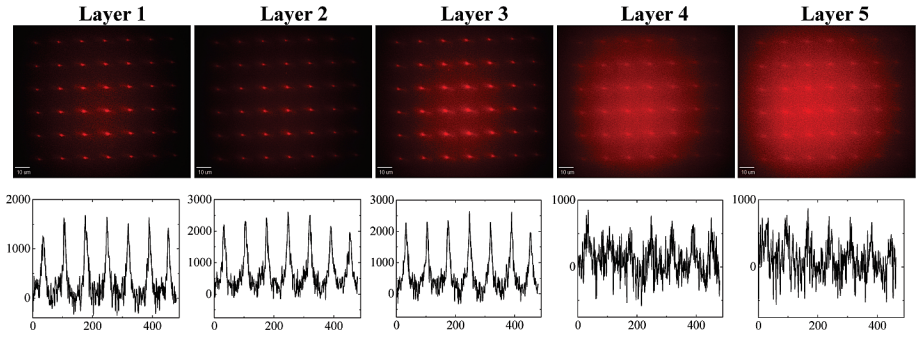

FIGURE 8. Photosensitive polymeric system used for 3D, two-photon ODS and one-photon readout. Composition (w/w): 2, 1%; 5, 5%; 19, 94%. Two-photon writing was performed at 730 nm (2.4 mW), 200 fs, 60 ms exposure/voxel with a 60×, 1.4 NA oil immersion objective. One-photon readout (upper) was performed, layer-by-layer (~0.4 μm/layer), with a modified TRITC filter cube (Ex:525/40; DM: 555; Em:624/40), with the same objective as that used for writing. Layers 1−5 show significant reduction of the signal-to-noise ratio (lower) in the fluorescence intensity scan for all of the layers. Scale bar: 10 μm.

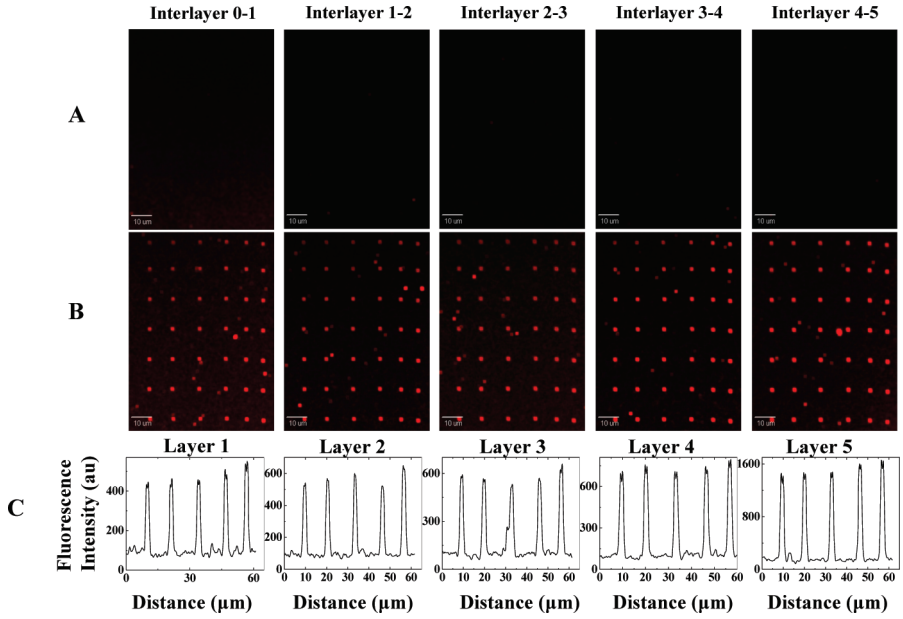

FIGURE 9. Photosensitive polymeric system used for 3D, two-photon ODS and two-photon reradout. Composition (w/w): 2, 1%; 5, 5%; 19, 94%. Two-photon writing was performed at 730 nm (2.4 mW), 200 fs, 60 ms exposure/voxel with a 60×, 1.4 NA oil immersion objective. Two-photon readout was performed, layer-by-layer (~0.4 μm/layer), at 860 nm (7 mW), 200 fs, with the same objective as that used for writing. (A) Blank interlayers (unrecorded volume between voxel layers). (B) Two-photon readout of five layers of recorded voxels. (C) Fluorescence intensity scan of each layer showing consistenly good signal-to-noise ratios throughout all five recorded layers of data. Note that because there is virtually no fluorescence signal in between the layers (A), the system is crosstalk-free. Scale bar: 10 μm.

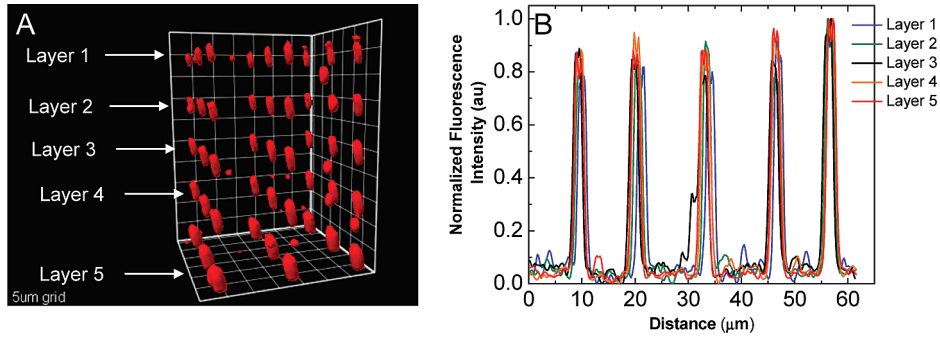

FIGURE 10. Photosensitive polymeric system used for 3D, two-photon ODS. Composition (w/w): 5, 5%; 2, 1%; 19, 94%. Two-photon writing was performed at 730 nm (2.4 mW), 200 fs, 60 ms exposure/voxel with a 60×, 1.4 NA oil immersion objective. Two-photon readout was performed, layer-by-layer (~0.4 mm/scaning), at 860 nm (7 mW), 200 fs, with same objective as that used for writing. (A) 3D image reconstruction done by overlaying all readout layers using SlideBook 4.1 (surface mode). (B) Normalized fluorescence intensity scan of all layers showing excellent signal-to-noise ratios throughout the entire polymer matrix. Note that because there is virtually no fluorescence signal in between the layers, the system is crosstalk-free. Scale: 5 μm grid.

sections and high fluorescence quantum yields. The structures of the 2PA PAGs proved to be very useful in this type of system and should also be of considerable value in systems in which photoacid generation by 2PA is of the

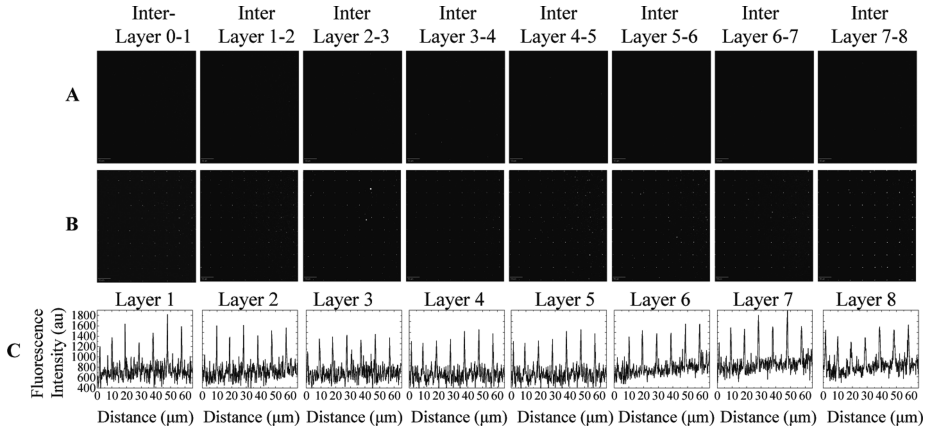

FIGURE 11. Photosensitive polymeric system used for 3D, two-photon ODS. Composition (w/w): 5, 5%; 2, 1%; 19, 94%. Two-photon writing was performed at 710 nm (1.6 mW), 200 fs, 60 ms exposure/voxel with a 60×, 1.4 NA oil immersion objective. Two-photon readout was performed, layer-by-layer (~0.4 mm/scaning), at 860 nm (9 mW), 200 fs, with the same objective as that used for writing. (A) Blank interlayers (unrecorded volume between voxel layers). (B) Two-photon readout of the eight layers. (C) Fluorescence intensity scan of each layer showing good signal-to-noise ratios throughout all eight recorded layers of data. Note that because there is virtually no fluorescence signal in between the layers (A), the system is crosstalk-free. Scale bar: 10 μm.

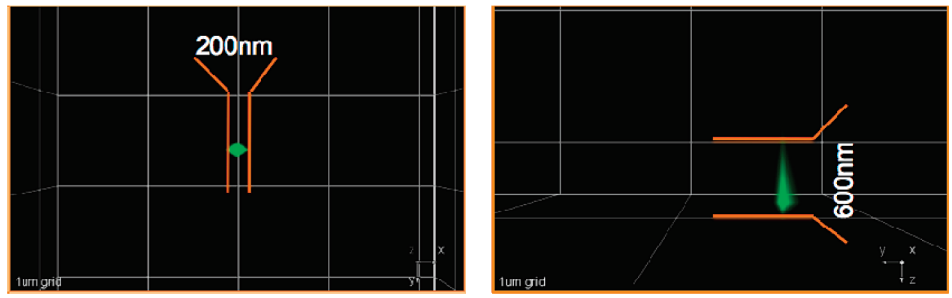

FIGURE 12. Photosensitive polymeric system used for 3D, two-photon ODS. Composition (w/w): 5, 5%; 2, 1%; 19, 94%. Two-photon writing was performed at 710 nm (1.6 mW), 200 fs, 60 ms exposure/voxel with a 60×, 1.4 NA oil immersion objective. Two-photon readout was performed, layer-by-layer (~0.4 mm/scaning), at 860 nm (9 mW), 200 fs, with same objective as that used for writing. This voxel represents an average voxel as determined by surveying the average size of the voxels in layers 3 and 4 of the eight-layer series. On the basis of these size features, we estimated the maximum storage capacity to be approximately 1.8 × 10^{13} bits/cm^3.

essence (i.e., 2PA microfabrication). These PAGs represent an important contribution to the very few sulfonium salt structures reported to generate photoacid upon 2PA (28, 29). Of the different polymer matrixes that were used as supports, **19** gave the best results because of its transparency and because it was a robust matrix in which the dyes and PAGs were generally very soluble. The photoinduced formation of a thiolene polymer matrix is, however, a feasible alternative in which one can easily obtain recording media of different mechanical and optical properties.

The 2PA WORM ODS system, consisting of 5 wt % PAG **5**, 1 wt % 2PA dye **2**, and 94 wt % host polymer **19**, proved to be resilient to overexposure, and the inherent nonlinearity and sensitivity of this system enabled multilayer recording and readout of crosstalk-free 3D optical data with subdiffraction-limited voxel sizes. The advantages of two-photon writing and readout were clearly demonstrated, providing a storage density capacity of 1.8 × 10^{13} bits/cm^3.

Acknowledgment. We acknowledge the National Science Foundation (Grants ECS-0621715 and CHE-0832622), the U.S. Civilian Research and Development Foundation (Grant UKB2-2923-KV-07), and the Ministry of Education and Science of Ukraine (Grant M/49-2008) for support of this work.

Supporting Information Available: Experimental characterization spectra of new molecules after purification (^{1}H and ^{13}C NMR) and an additional figure showing 3D image reconstruction of eight layers of two-photon recording and readout. This material is available free of charge via the Internet at http://pubs.acs.org.

REFERENCES AND NOTES

(1) van de Nes, A. S. B. J. M.; Pereira, S. F. *Rep. Prog. Phys.* **2006**, (69), 2323–2363.
(2) Strickler, J. H.; Webb, W. W. *Opt. Lett.* **1991**, *16* (22), 1780–1782.
(3) Corredor, C. C.; Huang, Z. L.; Belfield, K. D. *Adv. Mater.* **2006**, *18* (21), 2910–2914.
(4) Belfield, K. D.; Schafer, K. J. *Chem. Mater.* **2002**, *14* (9), 3656–3662.
(5) Dvornikov, A. S.; Rentzepis, P. M. *Opt. Commun.* **1997**, *136* (1–2), 1–6.
(6) Parthenopoulos, D. A.; Rentzepis, P. M. *Science* **1989**, *245* (4920), 843–845.
(7) Schafer, K. J.; Hales, J. M.; Balu, M.; Belfield, K. D.; Van Stryland, E. W. *J. Photochem. Photobiol., A* **2004**, *162* (2–3), 497–502.
(8) Belfield, K. D.; Schafer, K. J.; Mourad, W.; Reinhardt, B. A. *J. Org. Chem.* **2000**, *65* (15), 4475–4481.
(9) Belfield, K. D.; Morales, A. R.; Kang, B. S.; Hales, J. M.; Hagan, D. J.; Van Stryland, E. W.; Chapela, V. M.; Percino, J. *Chem. Mater.* **2004**, *16* (23), 4634–4641.
(10) Yanez, C. O.; Andrade, C. D.; Belfield, K. D. *Chem. Commun.* **2009**, 827–829.
(11) Belfield, K. D.; Wang, J. X. *J. Polym. Sci., A* **1995**, *33* (8), 1235–1242.

(12) Belfield, K. D.; Yao, S.; Morales, A. R.; Hales, J. M.; Hagan, D. J.; Van Stryland, E. W.; Chapela, V. M.; Percino, J. *Polym. Adv. Technol.* **2005**, *16* (2−3), 150–155.
(13) Bredereck, M. G. S.; Griebenow, W. *Chem. Ber.* **1973**, *106*, 3732.
(14) Yoshino, K.; Kohno, T.; Uno, T.; Morita, T.; Tsukamoto, G. *J. Med. Chem.* **1986**, *29* (5), 820–825.
(15) Zeng, D. X.; Chen, Y. *J. Photochem. Photobiol., A* **2007**, *186* (2−3), 121–124.
(16) Lakowicz, J. R. *Principles of Fluorescence Spectroscopy*; Kluwer Academic Publishers: New York, 1999.
(17) Pohlers, G.; Scaiano, J. C.; Sinta, R.; Brainard, R.; Pai, D. *Chem. Mater.* **1997**, *9* (6), 1353–1361.
(18) Belfield, K. D.; Bondar, M. V.; Yanez, C. O.; Hernandez, F. E.; Przhonska, O. V. *J. Mater. Chem.* **2009**, *19*, in press, DOI: 10.1039/b820950b.
(19) Dey, J. K.; Dogra, S. K. *Bull. Chem. Soc. Jpn.* **1991**, *64* (10), 3142–3152.
(20) Arnett, E. M.; Quirk, R. P.; Burke, J. J. *J. Am. Chem. Soc.* **1970**, *92* (5), 1260–1266.
(21) Belfield, K. D.; Bondar, M. V.; Przhonska, O. V.; Schafer, K. J.; Mourad, W. *J. Lumin.* **2002**, *97* (2), 141–146.
(22) Belfield, K. D.; Crivello, J. V. *Photoinitiated Polymerization*; Oxford University Press: Washington, DC, 2003.
(23) Denk, W.; Strickler, J. H.; Webb, W. W. *Science* **1990**, *248* (4951), 73–76.
(24) He, G. S.; Bhawalkar, J. D.; Zhao, C. F.; Park, C. K.; Prasad, P. N. *Opt. Lett.* **1995**, *20* (23), 2393–2395.
(25) Ehrlich, J. E.; Wu, X. L.; Lee, I. Y. S.; Hu, Z. Y.; Rockel, H.; Marder, S. R.; Perry, J. W. *Opt. Lett.* **1997**, *22* (24), 1843–1845.
(26) Belfield, K. D.; Bondar, M. V.; Przhonska, O. V.; Schafer, K. J. *Photochem. Photobiol. Sci.* **2004**, *3* (1), 138–141.
(27) Dektar, J. L.; Hacker, N. P. *J. Am. Chem. Soc.* **1990**, *112* (16), 6004–6015.
(28) Zhou, W. H.; Kuebler, S. M.; Braun, K. L.; Yu, T. Y.; Cammack, J. K.; Ober, C. K.; Perry, J. W.; Marder, S. R. *Science* **2002**, *296* (5570), 1106–1109.
(29) Zhou, W. H.; Kuebler, S. M.; Carrig, D.; Perry, J. W.; Marder, S. R. *J. Am. Chem. Soc.* **2002**, *124* (9), 1897–1901.

AM900587U